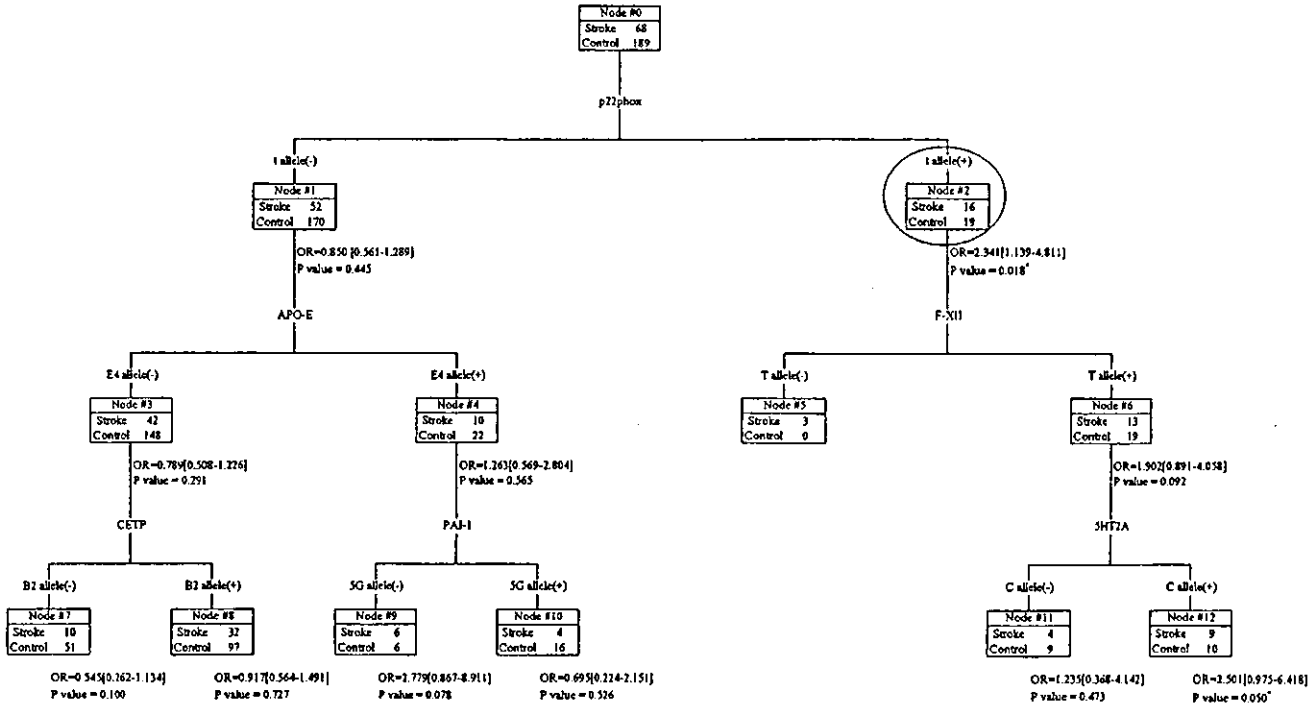

Fig. 2 Exact tree model #1 (p22phox). *Circle* statistically significant combination, *OR* odds ratio of each node to root node (Node #0) and its 95% confidence interval. $*P<0.05$, chi-square test

Fig. 3 Exact tree model #2 (APO-E). *Circle* statistically significant combination, *OR* odds ratio of each node to root node (Node #0) and its 95% confidence interval. $*P<0.05$ and $**P<0.01$, chi-square test

with a combination of APO-E E4 allele-positive, PAI-1 5G allele-negative and Mitochondria A allele-negative, the odds ratio became 6.49 (1.63–25.79). And in Node #11, with a combination of APO-E E4 allele-negative, CETP B2 allele-negative, and ACE I allele-positive, the qdds ratio became 0.41 (0.19–0.91), which can be a protective combination against stroke. In the same way, we can extract another one, three, and three statistically significant combinations from the tree models in Figs. 4, 5, and 6, respectively.

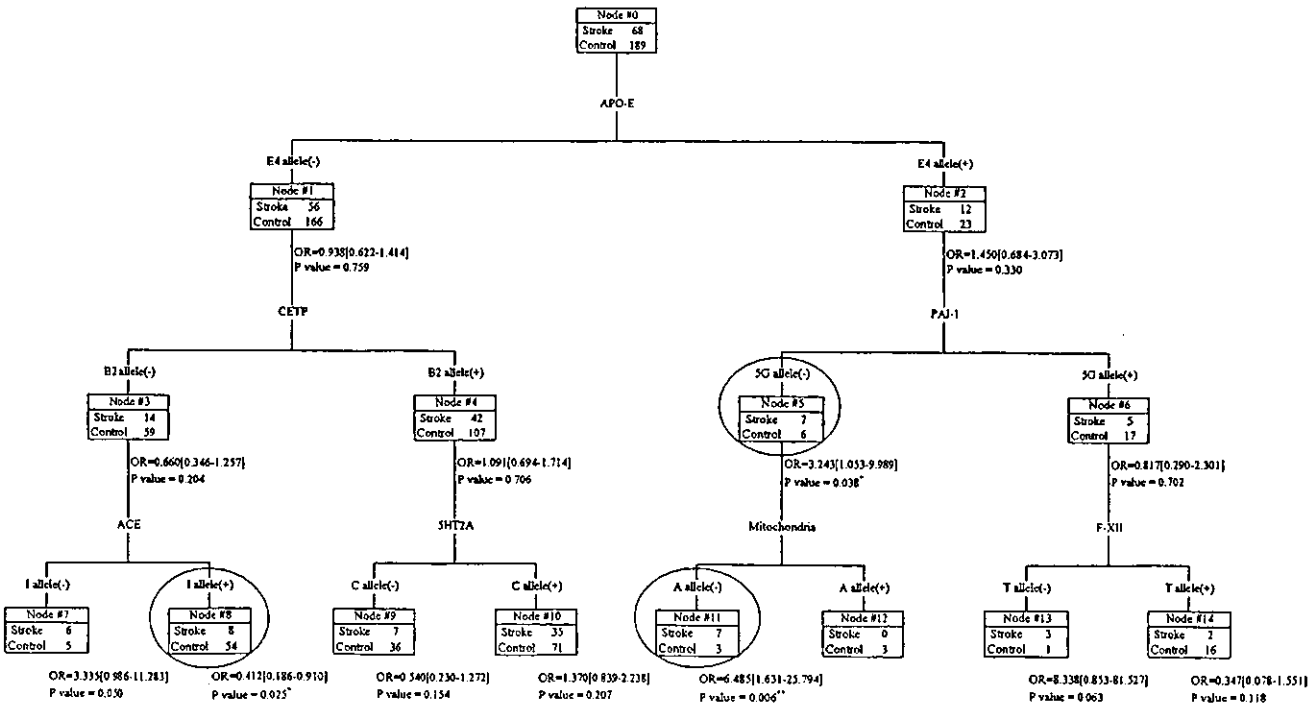

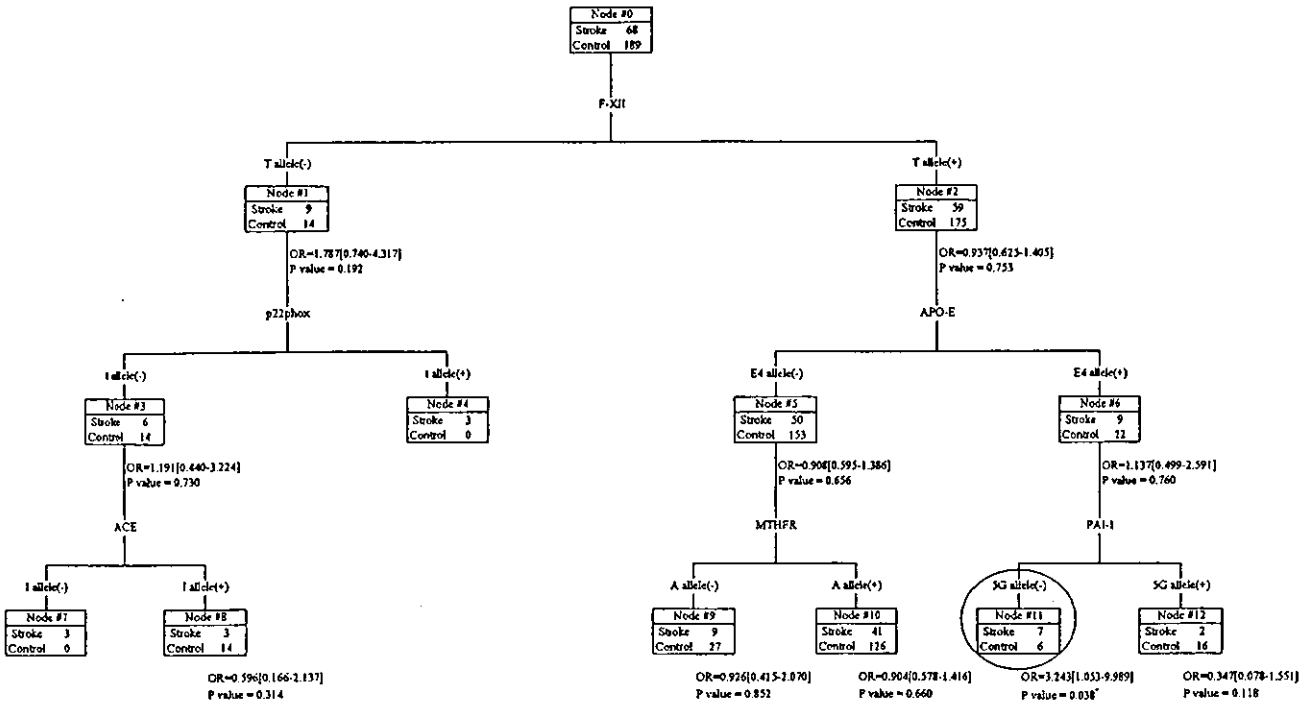

Fig. 4 Exact tree model #3 (F-XII). *Circle* statistically significant combination, *OR* odds ratio of each node to root node (Node #0) and its 95% confidence interval. $*P < 0.05$, chi-square test

Discussion

Although not shown in the Figures, we extended Nodes #7, #8, #9, and #10 in Fig. 2 (which are the same structure as Nodes #3, #4, #5, and #6 in Fig. 3) one more step down and found the same split in Nodes #7, #9, and #10. Node #8 was split by APO-E E2 allele instead of 5HT2A C allele. Because the left-side branch in Fig. 2 started from 222 subgroup [Node #1, p22phox t allele(−)], it is not surprising that the later splits are not

Fig. 5 Exact tree model #4 (ACE). *Circle* statistically significant combination, *OR* odds ratio of each node to root node (Node #0) and its 95% confidence interval. $*P < 0.05$ and $**P < 0.01$, chi-square test

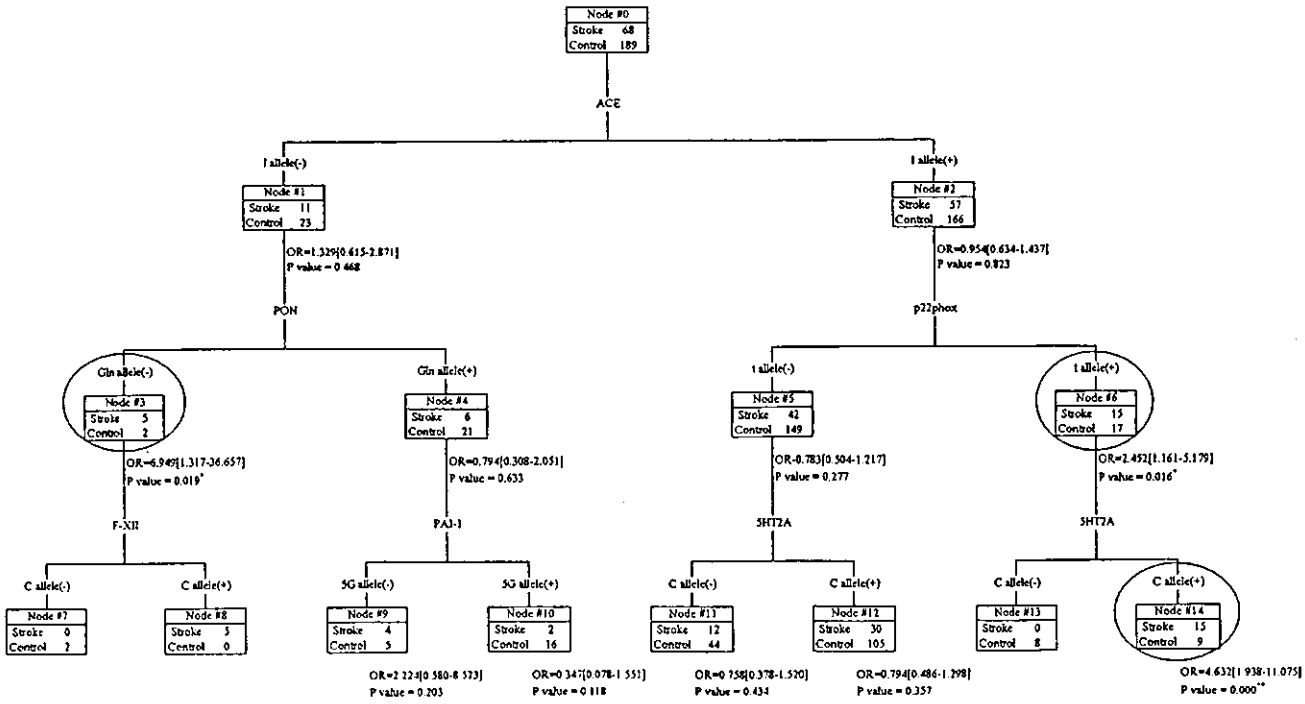

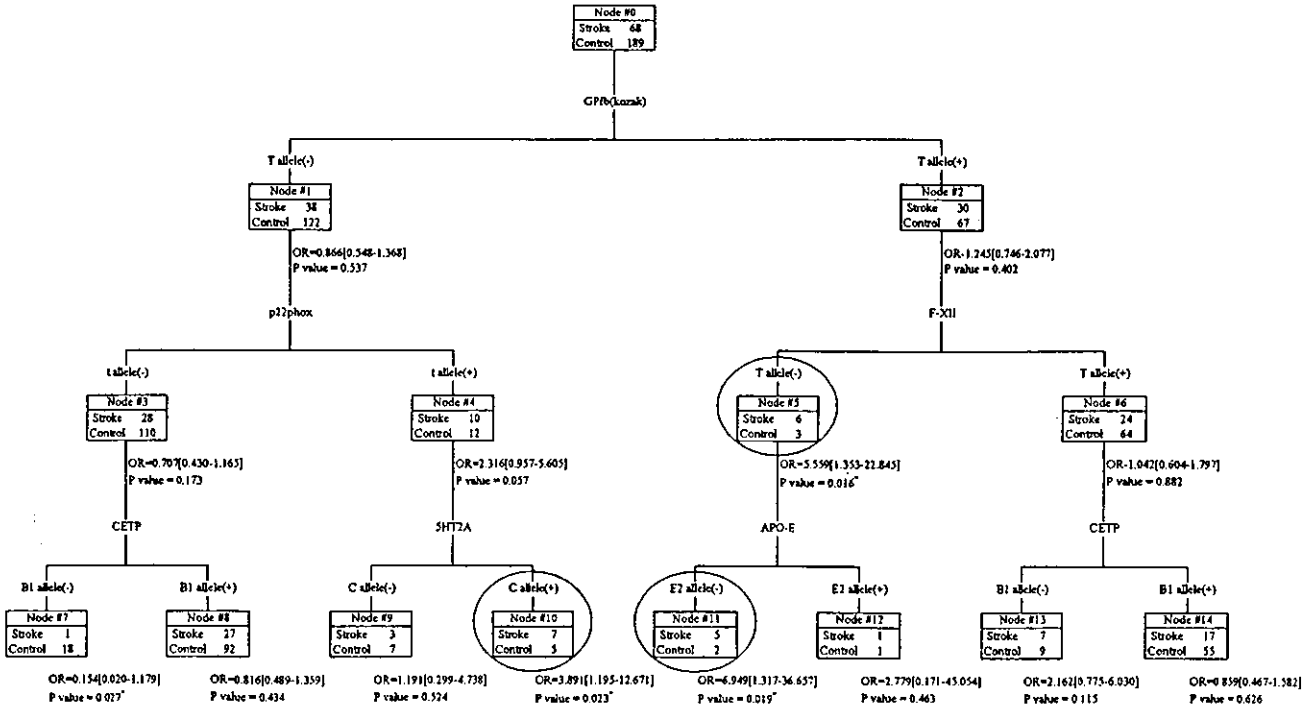

Fig. 6 Exact tree model #5 [GPIb (kozak)]. *Circle* statistically significant combination, *OR* odds ratio of each node to root node (Node #0) and its 95% confidence interval. $*P < 0.05$, chi-square test

Table 3 List of alleles used as variates for this analysis. Genetic polymorphism markers are listed in alphabetical order

Genetic polymorphism markers	Variates		
5HT2A	C allele	T allele	
ACE	D allele	I allele	
APO-E	E2 allele	E3 allele	E4 allele
CETP	B1 allele	B2 allele	
FIB-B	H1 allele	H2 allele	
F-XII	C allele	T allele	
GPIb (145Thr/Met)	M allele	T allele	
GPIb (kozak)	C allele	T allele	
Mitochondria	A allele	T allele	
MTHFR	A allele	V allele	
NOS	a allele	b allele	
P22phox	c allele	t allele	
PAI-1	4G allele	5G allele	
PON	Arg allele	Gln allele	

Table 4 List of acquired *P* values by Fischer's exact test in case-control tables. Genetic polymorphism markers are listed in ascending order by *P* value

Genetic polymorphism markers	Variates	*P* values
P22phox	t allele*	0.012
APO-E	E4 allele*	0.031
F-XII	T allele	0.056
ACE	I allele	0.112
GPIb (kozak)	T allele	0.220
PAI-1	5G allele	0.506
Mitochondria	A allele	0.541
FIB-B	H1 allele	0.611
PON	gln allele	0.654
GPIb (145Thr/Met)	M allele	0.707
CETP	B2 allele	0.756
NOS	a allele	0.840
MTHFR	A allele	0.849
5HT2A	C allele	0.863

* $P < 0.05$, Fischer's exact test between stroke patients and healthy controls

completely consistent with the result from 257 whole population cases. When a similar structure was observed such as between Fig. 3 and the left-side branch in Fig. 2, we could speculate the root split (p22phox t allele in this case) influence little on the later splits. However, it does not mean the root split is unnecessary for making the tree, since the other side branch can be meaningful (unfortunately meaningless in this case). Such a consideration can be made because the number of tree models is plural in the exact tree method. Regular decision tree algorithm makes only one tree, and structural similarity cannot be evaluated. This is one of the strong points the exact tree algorithm has over the regular decision tree algorithm.

As shown in Fig. 1, 5HT2A did not show a high score (i.e., low *P* value) by itself, but was useful for making trees (Figs. 2, 3, 5, 6). It is speculated that this polymorphism has a low risk by itself but has a high risk when combined with the other polymorphisms. Such a combination is the main target the exact tree method aims for.

From the same population, the allele frequencies observed can differ in each sampling time. However,

these differences can be controlled within reasonable statistical error rates. Of course even statistically significant combinations may contain some false positives, but this problem might be out of scope of exploratory methods by nature. Other verificatory approaches are needed for explored hidden combinations, and the exact tree method will work efficiently in the former steps.

In this paper, we adopted the P value of Fischer's exact test as the splitting criterion for the decision tree. This splitting criterion can be substituted for the chi-square of CHAID (Kass 1980), the improvement score of CART (Breiman et al. 1980), the gain ratio of C4.5 (Quinlan 1993), and so on, by using the exact tree method we proposed. We have already tested the effectiveness of the exact tree method with the odds ratio as the splitting criterion (data not shown). It is impossible to state which splitting criterion is the best in decision tree modeling, because the each criterion is the best in each mathematical modeling theory. So we adopted the P value of Fischer's exact test because it is easily interpreted as the probability and is familiar to biologists and medical researchers. Moreover, we can use the commonly used alpha error rate (0.05 or 0.01) as the standard for judging the magnitude of the value.

Here we need to clarify the advantage of the exact tree method over the regular decision tree method. If we adopt the regular decision tree method, we can get the best (i.e., only one) classification tree model (Fig. 2). On the contrary, the exact tree method makes plural tree models, including the best classification tree model (Figs. 2, 3, 4, 5, 6). In the real data analysis, while the regular decision tree shows us no significant combination (Fig. 2), five tree models constructed by the exact tree method showed us ten significant combinations (Figs. 2, 3, 4, 5, 6). Because the output of the exact tree method always includes the best tree model, it is never inferior to the regular decision tree method as to the extraction of hidden significant combinations. In addition, the amount of computation increases not exponentially but only several times from that of regular decision tree analysis. That is why we report this new method as an efficient and feasible exploratory technique for handling such large-scale genomic data as round-robin approach, which otherwise is impossible.

For reference, we executed the logistic regression analysis in which 14 polymorphisms are incorporated as independent variables. APO-E E4 allele and Factor XII gene t allele are statistically significant polymorphisms by both compulsory and stepwise methods. In the exact tree method, these two polymorphisms are selected as the first splitting variables in Figs. 3 and 4, and four statistically significant combinations are extracted. Regular decision tree method failed to find any combinations of the two polymorphisms above. This finding supports the advantage of the exact tree method over regular decision tree methods.

Since this method is an exploratory screening method, we do not insist that the individual results are solid evidences by themselves. We want to emphasize our success in extracting combinations of three polymorphisms using real genetic data. From the obtained tree models, we succeeded in extracting ten statistically significant combinations that may elevate or decrease the risk of stroke.

Here we handle a very small data set (only 14 genetic markers) in this pilot analysis, since round-robin explorations of multiple combinations are executable in ordinary computer workstations. So the advantage of the exact tree method is obscure, but the situation will change in handling extremely large-scale data set. For example, when we handle 100,000 genetic markers, which can be real in some whole genome approach researches, we need 10,000,000,000 operations to check all the combinations of two markers. In this situation, we need 1,000,000,000,000,000 operations to check all the combinations of three markers. Such an acute increase of the amount of computation at an exponential rate makes it impossible to extract combinations of large numbers of markers. With this new data mining method, however, the increase of the amount of computation is not exponential, and it can extract multiple combinations efficiently without computational explosion.

To assess the degree of the reduction in calculation task quantitatively, we did the reduction rate estimation trial. Suppose the number of genetic polymorphisms is N and we want to know the statistically significant disease-associated combinations of three polymorphisms. In the round-robin approach, we need to execute chi-square test $N \times (N-1) \times (N-2)$ times. On the other hand, the 3-step splitting exact tree method (i.e., the depth of the tree is 4) demands $3 \times n \times N$ times, where n is the number of tree models we make, which is less than N and usually less than 10. So the degree of the reduction in calculation task is evaluated as $\frac{3 \times n \times N}{N \times (N-1) \times (N-2)}$ and this reduction ratio simply decreases as N increases. And the number of tree models (n) is usually rather smaller than the total number of polymorphisms in consideration (N), this reduction ratio decreases exponentially. In spite of the rather small number of polymorphisms we demonstrated in this paper ($N=14$, $n=5$), this reduction rate is estimated to be 0.096. This estimation suggests the exact tree method works effectively enough in handling rather small genetic data, and this efficiency will increase when handling larger data. This new data mining method will facilitate the extraction of combinations from the huge genetic data that we are now confronted with and may provide a good foothold for further verificatory research.

Appendix

The exact probability of observing a table with cells (a, b, c, d) is
when

$$P(a,b,c,d) = \frac{{}_{m_1}C_a \cdot {}_{m_2}C_b}{{}_{N}C_{n_1}} = \frac{n_1!n_2!m_1!m_2!}{N!} \frac{1}{a!b!c!d!}$$

	Disease (+)	Disease (−)	
Polymorphism (+)	a	b	n_1
Polymorphism (−)	c	d	n_2
	m_1	m_2	N (total)

This probability distribution is known as the hypergeometric distribution (Bernard 2000).

Suppose the probability that a man had polymorphism (+) given that he had disease (+) $=p_1$, and the probability that a man had polymorphism (+) given that he had disease (−) $=p_2$. Here we wish to test the hypothesis H_0: $p_1=p_2$ versus H_1: p_1 not $=p_2$.

General procedure and computation of P value using Fischer's exact test are as follows:

1. Enumerate all possible tables with the same row and column margins (i.e., n_1, n_2, m_1, m_2) as the observed table
2. Compute the exact probability of each table enumerated in previous step
3. Suppose the observed table is the x table and the last table enumerated is the k table. To test the hypothesis H_0: $p_1=p_2$ versus H_1: $p_1<p_2$, the P value is computed as $P(0)+P(1)+\cdots+P(x)$ (left-hand tail area). To test the hypothesis H_0: $p_1=p_2$ versus H_1: $p_1>p_2$, the P value is computed as $P(x)+P(x+1)+\cdots+P(k)$ (right-hand tail area). To test the hypothesis H_0: $p_1=p_2$ versus H_1: p_1 not $=p_2$, the P value is computed as $2\times\min[P(0)+P(1)+\cdots+P(x), P(x)+P(x+1)+\cdots+P(k), 0.5]$.

This P value can be interpreted as the probability of obtaining a table as extreme as the observed table.

References

Ad Hoc Committee of National Institute of Neurological Disorders and Stroke (1990) Classification of cerebrovascular disease III. Stroke 21:637–676

Bernard R (2000) Fundamentals of biostatistics, 5th edn. Duxbury, Pacific Grove

Breiman L, Friedman JH, Olshen RA, Stone CJ (1980) Classification and regression trees. Wadsworth, Belmont

Ishii K, Murata M, Oguchi S, Takeshita E, Ito D, Tanahashi N, Fukuuchi Y, Saitou I, Ikeda Y, Watanabe K (2004) Genetic risk factors for ischemic cerebrovascular disease of candidate prothrombotic gene polymorphisms in the Japanese population. Rinsho Byori 52:22–27

Ito D, Tanahashi N, Murata M, Sato H, Saito I, Watanabe K, Fukuuchi Y (2002) Notch3 gene polymorphism and ischemic cerebrovascular disease. J Neurol Neurosurg Psychiat 72:382–384

Kass G (1980) An exploratory technique for investigating large quantities of categorical data. Appl Stat 29:119–127

Miyaki K, Takei I, Watanabe K, Nakashima H, Watanabe K, Omae K (2002) Novel statistical classification model of type 2 diabetes mellitus patients for tailor-made prevention using data mining algorithm. J Epidemiol 12:243–248

Oguchi S, Ito D, Murata M, Yoshida T, Tanahashi N, Fukuuchi Y, Ikeda Y, Watanabe K (2000) Genotype distribution of the 46C/T polymorphism of coagulation factor XII in the Japanese population: absence of its association with ischemic cerebrovascular disease. Thromb Haemost 83:178–179

Quinlan JR (1993) C4.5: Programs for machine learning. Morgan Kaufmann, Los Altos

Sonoda A, Murata M, Ito D, Tanahashi N, Oota A, Tada-Yatabe Y, Takeshita E, Yoshida T, Saito I, Yamamoto M, Ikeda Y, Fukuuchi Y, Watanabe K (2000) Association between platelet glycoprotein Ibα genotype and ischemic cerebrovascular disease. Stroke 31:493–497

Journal of Cerebral Blood Flow & Metabolism
24:993–1003 © 2004 The International Society for Cerebral Blood Flow and Metabolism
Published by Lippincott Williams & Wilkins, Baltimore

Fluorometric Determination of Glucose Utilization in Neurons *in Vitro* and *in Vivo*

Yoshiaki Itoh, Takato Abe, Rie Takaoka, and Norio Tanahashi

From the Department of Neurology, Keio University School of Medicine, Shinjuku, Tokyo, Japan

Summary: Glucose is the major energy source the adult brain utilizes under physiologic conditions. Recent findings, however, have suggested that neurons obtain most of their energy from the oxidation of extracellular lactate derived from astroglial metabolism of glucose transported into the brain from the blood. In the present studies we have used 2-[N-(7-nitrobenz-2-oxa-1,3-diazol-4-yl)amino]-2-deoxy-D-glucose (2-NBDG), a fluorescent analogue of 2-deoxyglucose, which is often used to trace glucose utilization in neural tissues, to examine glucose metabolism in neurons *in vitro* and *in vivo*. Cultured neurons and astroglia were incubated with 2-NBDG for up to 15 minutes, and nonmetabolized 2-NBDG was washed out. We found that fluorescence intensity increased linearly with incubation time in both neurons and astroglia, indicating that both types of brain cells could utilize glucose as their energy source *in vitro*. To determine if the same were true *in vivo*, Sprague-Dawley rats were injected intravenously with a pulse bolus of 2-NBDG and decapitated 45 minutes later. Examination of brain sections demonstrated that phosphorylated 2-NBDG accumulated in hippocampal neurons and cerebellar Purkinje cells, indicating that neurons can utilize glucose *in vivo* as energy source. **Key Words:** 2-deoxyglucose—2-NBDG—Glucose utilization—Neuron—Astroglia—Fluorescence.

Glucose is the main and essential substrate for energy metabolism in the adult brain under physiologic conditions (Clarke and Sokoloff, 1999). Its metabolic pathway consists of two sequential processes, first by glycolysis to pyruvate/lactate in the cytosol, followed by oxidation in the mitochondria to CO_2 and H_2O. On the basis mainly of studies with cultured neurons and astroglia, it has been proposed that these glycolytic and oxidative components are compartmentalized between astroglia and neurons respectively (Magistretti and Pellerin, 1999; Pellerin et al., 1998). The extent of this partition is, however, controversial; some suggest that it is partial (Itoh et al., 2003*a*,*b*) and others that it is complete (Sibson et al., 1998). The purpose of the present study was to evaluate the degree of the proposed compartmentalization of glycolysis between astroglia and neurons *in vivo*.

Autoradiographic measurement of local cerebral glucose utilization with radioactive 2-deoxyglucose is a well-established method and is widely used to evaluate energy metabolism in the brain (Sokoloff et al., 1977). Intravenously injected 2-[^{14}C]deoxyglucose is transported into the brain and phosphorylated by hexokinase in the brain cells. There is very little glucose-6-phosphatase activity to hydrolyze glucose-6-phosphate in neurons or astroglia (Dienel et al., 1988; Gotoh et al., 2000), and, therefore, the rates of 2-[^{14}C]deoxyglucose phosphorylation can be determined from the accumulation of the isotope within the tissues, measured by quantitative autoradiography, and the time courses of the arterial plasma 2-[^{14}C]deoxyglucose and glucose concentrations (Sokoloff et al., 1977). The rates of glucose utilization are subsequently calculated from the rates of 2-[^{14}C]deoxyglucose phosphorylation and a proportionality constant that encompasses the ratios of the kinetic constants of 2-[^{14}C]deoxyglucose and glucose for blood-brain barrier transport and phosphorylation by hexokinase (Sokoloff et al., 1977). The autoradiographic 2-[^{14}C]deoxyglucose method, however, has too limited spatial resolution to distinguish between neurons and astroglia.

Recently, 2-[N-(7-nitrobenz-2-oxa-1,3-diazol-4-yl)amino]-2-deoxy-D-glucose (2-NBDG), a fluorescent analogue of 2-deoxyglucose, has become available (Yoshioka et al., 1996*b*) and has been used to assess glucose transport in vascular smooth muscle cells (Lloyd et al., 1999), *Escherichia coli* (Natarajan and Srienc, 2000; Yoshioka et al., 1996*b*), astrocytes (Loaiza et al., 2003), cardiomyocytes (Ball et al., 2002), enterocytes

Address correspondence to Yoshiaki Itoh, Department of Neurology, Keio University School of Medicine, Shinanomachi 35, Shinjuku, Tokyo, 160–8582, Japan; e-mail: yoshiito@sc.itc.keio.ac.jp

DOI: 10.1097/01.WCB.0000127661.07591.DE

(Román et al., 2001), yeast Candida albicans (Yoshioka et al., 1996*a*), and pancreatic β-cells (Yamada et al., 2000). In the present study, we first validated the usefulness of 2-NBDG as a fluorescent tracer to trace glucose utilization in cultured neurons and astroglia and then applied it in studies in whole animals. The results showed that neurons in the brain utilize glucose as a substrate for energy metabolism, thus corroborating previous reports suggesting that neurons *in vivo* utilize glucose in addition to lactate provided by astroglia (Itoh et al., 2003*a*,*b*).

MATERIALS AND METHODS

Materials

Chemicals and materials were obtained from the following sources: 2-NBDG, and Texas red goat anti-mouse IgG antibody from Molecular Probes Inc (Eugene, OR, U.S.A.); high-glucose (25 mM) Dulbecco's modified Eagle medium (DMEM), penicillin, and streptomycin from Life Technologies (Gaithersburg, MD, U.S.A.); defined fetal bovine serum (FBS) from HyClone Laboratories (Logan, UT, U.S.A.); trypsin-EDTA from Boehringer Mannheim (Indianapolis, IN, U.S.A.); Dulbecco's phosphate buffered saline (PBS), Hanks' Balanced Salt Solution (HBSS), poly-L-lysine, cytosine arabinoside, monoclonal anti-calbindin-D-28K antibody, monoclonal anti-glial fibrillary acidic protein (GFAP) antibody, and monoclonal anti-Neurofilament 68-kDa antibody from Sigma (St. Louis, MO, U.S.A.); anti-vimentin antibody from Roche Molecular Biochemicals; anti-NeuN antibody and monoclonal antibodies against Neurofilament 160-kDa from Chemicon (Temecula, CA, U.S.A.); and sodium pentobarbital from Dainippon Pharmaceutical (Tokyo, Japan).

Animals

All procedures on animals were in accordance with *The Animal Experimental Guideline of Keio University School of Medicine* and approved by the Experimental Committee of Keio University. Cell cultures were prepared from timed pregnant Sprague-Dawley rats (Japan SLC, Hamamatsu, Japan). *In vivo* glucose utilization studies were carried out in normal adult male 350–400 g Sprague-Dawley rats (Charles River, Yokohama, Japan), maintained on a 12-hour light/dark cycle with humidity and temperature controlled at normal levels and allowed food and water *ad libitum*.

Cell cultures

Neuronal and astroglial cultures were prepared from mesencephalon of fetal rats on embryonic day 16. The mesencephalon was excised and, after removal of meninges and blood vessels, mechanically disrupted by gentle passage through a 22-gauge needle. Neuronal cultures were prepared by dispersion of the dissociated cells (1.5×10^6 cells per mL) in poly-L-lysine-coated 35-mm glass-bottom dishes (Matsunami, Japan) and incubation in high-glucose (25 mM) DMEM containing 10% (vol/vol) FBS, penicillin (100 units/mL), and streptomycin (100 μg/mL) at 37°C in humidified air containing 7% CO_2. After 3 days of incubation, cytosine arabinoside (20 μM) was added to the culture medium. Assays were done on 8-day-old cultures. Astroglial cultures were prepared by dispersion of the dissociated cells (5×10^5 cells per mL) in uncoated 35-mm glass-bottom dishes and incubation under the same conditions, except no cytosine arabinoside was added, and the culture medium was changed on day 2 and every third day thereafter. Assays were done on 15-day-old cultures.

Some cells from the neuronal and astroglial cultures were plated in six-well culture plates for immunohistological examination. Neurons were stained with monoclonal antibodies against Neurofilament 68-kDa (Sigma) and 160-kDa (Chemicon) proteins. Astroglia were identified by GFAP and vimentin. More than 99% of the cells in the cultures showed the immunohistological character of the targeted cells.

Glucose utilization in cultured neurons and astroglia

The use of radioactive 2-deoxyglucose to determine glucose utilization in cultured brain cells has been described in detail (Brookes and Yarowsky, 1985) and well validated (Gotoh et al., 2000). To overcome the limitations in spatial resolution associated with autoradiography, fluorescent 2-NBDG was used in place of 2-[^{14}C]deoxyglucose. After 15 minutes of preincubation with HBSS containing 2 mM glucose in air/5% CO_2, the preincubation medium was replaced by HBSS with 2 mM glucose containing one of six concentrations of 2-NBDG (0, 10, 30, 50, 70, and 90 μM), and incubation was continued for either 0, 5, 10, 15, or 20 minutes. At the end of the incubation, the reaction mixture was replaced by fresh HBSS with 2 mM glucose, and incubation was continued for 5 minutes to allow efflux of residual nonphosphorylated 2NBDG from the cells. The cell carpets were washed three times with HBSS containing 2 mM glucose.

Fluorescence imaging was obtained with a fluorescence microscopy system, which consisted of an inverted microscope (TE2000, Nikon, Japan), a Xe arc lamp (C6979, Hamamatsu Photonics, Japan), a charge-coupled device (CCD) camera (C4742–95, Hamamatsu Photonics, Japan), and imaging software (Aquacosmos, Hamamatsu Photonics, Japan). Excitation light and emission light wave-lengths were set at 475 nm and 535 nm, respectively, by means of a filter set (XF100–2, Omega Optical, U.S.A.). Fluorescence intensity of standardized concentrations of 2NBDG, each of which filled a culture dish without cells, was measured for calibration. To minimize artifacts derived from photo bleaching and to enable comparisons of fluorescence intensities among different dishes, a series of measurement was performed continuously.

Glucose utilization in cultured neurons in each dish was calculated by averaging fluorescence intensity in a single visual field with a magnification of 10×. Thirty consecutive visual fields were evaluated to determine the mean fluorescence intensity for each dish. The fluorescence intensity was calibrated by setting the intensity obtained from 2 mL of 50 nM 2-NBDG in a culture dish without cells at 100 units.

Glucose utilization in cultured astroglia was measured in the same way as for neurons except that region of interest to measure fluorescence was set as a whole visual field obtained with a 20× objective lens. Fluorescence intensity of each image was calibrated in the same way.

Local cerebral glucose utilization *in vivo*

Rats were prepared for determination of local cerebral glucose utilization by insertion of PE50 catheters (Clay-Adams, NJ, U.S.A.) into a femoral artery and femoral vein under isoflurane anesthesia (5% for induction and 1.0–1.5% for maintenance in 70% N_2O/30% O_2). Lidocaine ointment (5%) was applied to the surgical wounds after closure, and loose-fitting plaster casts were applied to the animals' lower torsos to minimize locomotion. Body temperature was monitored and maintained at 37°C throughout the procedure. At least 3 hours were

allowed for recovery from surgery and anesthesia before initiation of determinations of glucose utilization.

Cerebral glucose utilization was determined in six rats by a fluorometric deoxyglucose method based upon the quantitative autoradiographic 2-[^{14}C]deoxyglucose method (Sokoloff et al., 1977). Either 2.5 μmol/kg or 25 μmol/kg of 2NBDG was intravenously injected as a bolus, and 45 minutes later the rats were injected with a lethal dose of pentobarbital. The brains were rapidly removed, frozen in isopentane maintained at −40° to −50°C with dry ice, and cut into 20-μm sections in a cryostat at −22°C. The frozen brain sections were thaw-mounted on glass cover-slips and immediately dried on a hot plate at approximately 60°C, and fluorescent images were obtained with the same fluorescence system as was used for the *in vitro* fluorescence studies described previously.

Additional *in vivo* studies were performed in four rats with 2-NBDG administered intracisternally to overcome the limited transport of 2-NBDG across the blood-brain barrier. In these studies, a silastic catheter (0.012-inch inner diameter × 0.025-inch outer diameter) (Read Plastic, Rockville, MD, U.S.A.) was inserted into the cisterna magna, and 2-NBDG, dissolved in artificial cerebrospinal fluid at a concentration of 15 μmol/mL, was infused continuously at a rate of 2.0 μL/min for 60 minutes. The intracisternal infusion was then discontinued, and 60 minutes were allowed for the washout of nonphosphorylated 2-NBDG from the tissues by transport and the circulation. The brain was then removed, frozen in isopentane, cut into 20-μm sections, and examined by fluorescence microscopy.

Immunohistochemistry of the brain sections

After fluorescent images of the 2-NBDG distribution were obtained, the same brain sections were processed for immunohistochemistry to identify the brain cells. The sections were immersed in PBS for 5 minutes, and the PBS was then replaced with fresh PBS. This washing with PBS was repeated three times to remove completely the fluorescent dye from the tissues. After application of 1.5% skim milk for 60 minutes, antibodies to either NeuN (1:200), Calbindin (1:3000) or GFAP (1:400) were placed on the sections, and the sections were kept at 4°C overnight. After three repeated 10-minute washouts, secondary antibody, that is, goat anti-mouse antibody conjugated with Texas-Red (1:400), was applied. After 2 hours of exposure to the antibody, 10-minute washouts were repeated, and the sections were mounted with a fluorescence mounting medium and observed with the fluoroscope.

To facilitate identification of the fluorescent sections, corresponding sections were obtained from independent rats and stained with cresyl violet.

RESULTS

Glucose utilization in cultured neurons and astroglia

Representative images of phosphorylated 2-NBDG in neurons are shown in Fig. 1. After incubation with 50 μM 2-NBDG for either 0 (A), 5 (B), 10 (C), 15 (D), or 20 (E) min, the nonphosphorylated 2-NBDG was washed out, and fluorescence intensity derived from phosphorylated 2-NBDG in neurons was found to increase with increasing incubation time (Fig. 1). Average fluorescence intensity for each incubation time was measured. Duplicate dishes were used for each incubation time, and values are expressed as means ± SD (graph in Fig. 1). Fluorescence intensity increased proportionately to incubation time. In some dishes, fluorescence intensity was followed intermittently for additional 60 or more minutes, and during that time fluorescence intensities did not decrease, confirming that the fluorescent tracer remaining in the cells was phosphorylated and trapped.

Similar assays were carried out with the 2-NBDG method in astroglia, and these provided images of phosphorylated 2-NBDG in astroglia (Fig. 2). After incubation of astroglia with 50 μM 2-NBDG for either 0 (A), 5 (B), 10 (C), 15 (D), or 20 (E) minutes, nonphosphorylated 2-NBDG was washed out. As found in the neurons, fluorescence intensity derived from phosphorylated 2-NBDG also increased with incubation time in the astroglia. Average fluorescence intensity for each incubation time was measured. Triplicate dishes were used for each incubation time, and values are expressed as means ± SD (graph in Fig. 2). Fluorescence intensity increased proportionately with incubation time in the astroglia as in the neurons. The effects of 2-NBDG concentration in the reaction mixture on 2-NBDG phosphorylation were also examined in astroglia. Astroglia were incubated with 0, 10, 30, 50, 70, or 90 μM 2-NBDG for 15 minutes followed by the washout of nonphosphorylated 2-NBDG as described previously. Fluorescence intensity in 30 consecutive visual fields was measured. Values are expressed as means ± SD (Fig. 3). Fluorescence intensity increased in proportion to the concentration of 2-NBDG in the reaction mixture, suggesting that hexokinase, the enzyme catalyzing the phosphorylation, is far from saturation in this range of concentration. (*i.e.*, <90 μM).

These incubation time and concentration dependencies that we observed indicate that the 2-NBDG is a useful fluorescent tracer with which to assay and localize glucose utilization in neurons and astroglia *in vitro*.

Local cerebral glucose utilization *in vivo*

A number of physiologic variables, including body temperature and arterial blood pressure, PCO_2, PO_2, and pH were monitored in those experiments in which glucose utilization was determined *in vivo*. None of these was found to change significantly during the procedure.

After fluorescence images for 2-NBDG were obtained from them, the tissue sections were washed out to remove phosphorylated 2-NBDG and then immunostained for histochemistry. Definitive images were obtained only with the high dose of 2-NBDG (25 μmol/kg). Figure 4 shows coronal brain sections at the level of hippocampus. Panels A to F demonstrate fluorescent images at the CA3 region of hippocampus. The region of observation is indicated with a square in panel G, which shows a section stained with cresyl violet. Panel A shows phosphorylated 2NBDG fluorescence in the pyramidal cell layer. A closer examination reveals that the majority of the fluorescence is located over cell bodies. Panel B shows anti-NeuN positive pyramidal neurons in CA3.

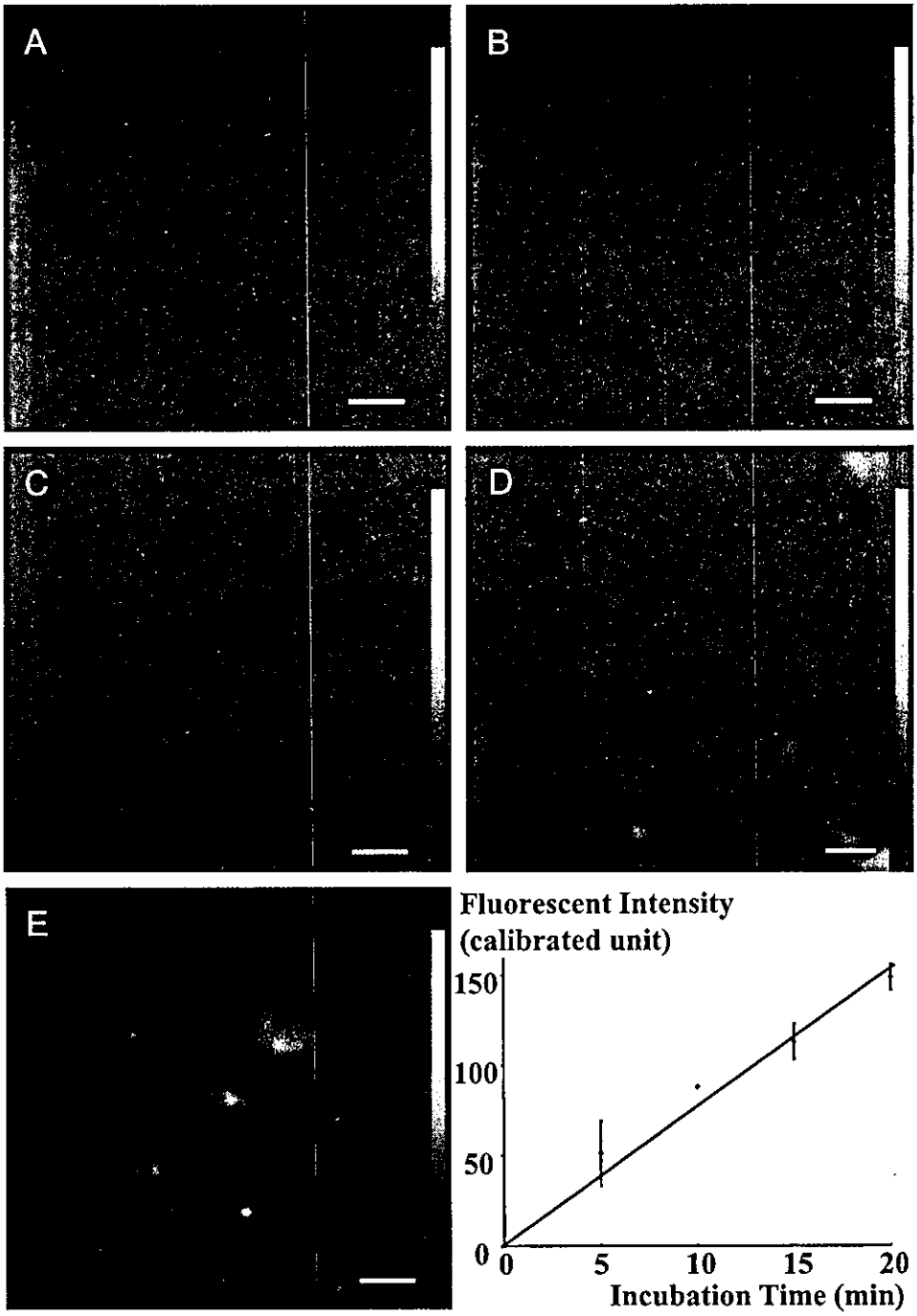

FIG. 1. Phosphorylation of 2-NBDG in neurons. After incubation of neurons with 2-NBDG for either 0 (A), 5 (B), 10 (C), 15 (D), or 20 minutes (E), the residual unmetabolized dye was washed out. Fluorescence intensity derived from phosphorylated 2-NBDG in the neurons increases with the incubation time. Scale bars = 100 μm. The graph shows phosphorylation of 2-NBDG in neurons. Fluorescence intensity derived from phosphorylated 2-NBDG in neurons increases proportionately with incubation time. Values are expressed as means ± SD.

Panel C is a superimposed image of panels A and B, showing high agreement (yellow regions) in distribution and morphology between 2-NBDG-accumulated cells and NeuN positive neurons. Arrows in these panels indicate some of the double-labeled cells. Artifacts such as the one in panels A, B, and C (thick arrow) were used to construct overlay of 2-NBDG images and immunohistochemical images.

Panel F in Fig. 4 is a superimposed image of panels D (2-NBDG image) and E (GFAP staining). GFAP-positive astroglia appear to constitute part of the cells with high accumulation of phosphorylated 2-NBDG. These cells shown in yellow (arrow) in panel F, however, are small in number, sparse in distribution, and different in morphology as compared with cells with 2-NBDG accumulation. Minor, if any, involvement of astroglia in overall 2-NBDG accumulation in panel F is distinct compared with the predominant neuronal involvement shown as high agreement of 2-NBDG-accumulated cells and NeuN positive neurons in panel C.

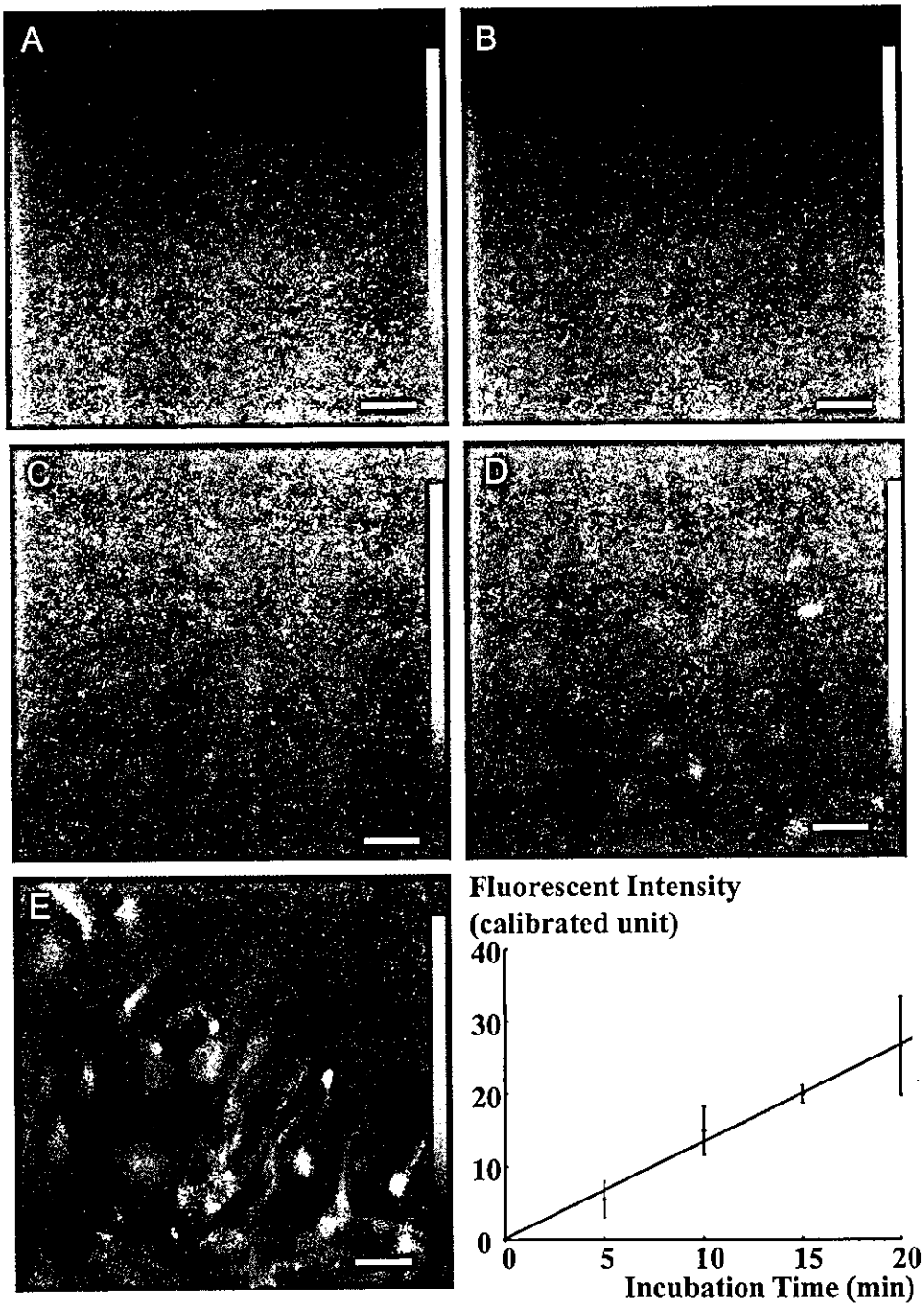

FIG. 2. Phosphorylation of 2-NBDG in astroglia. After incubation of astroglia with 2-NBDG for either 0 (A), 5 (B), 10 (C), 15 (D), or 20 (E), the residual unmetabolized dye was washed out. Fluorescence intensity derived from phosphorylated 2-NBDG in the astroglia increases with the incubation time. Scale bars = 50 μm. The graph shows phosphorylation of 2-NBDG in astroglia. Fluorescence intensity derived from phosphorylated 2-NBDG in the astroglia increases proportionately with incubation time. Values are expressed as mean ± SD.

These results clearly demonstrate that neurons mainly take up and phosphorylate glucose in the pyramidal cell layer of hippocampus and that astroglial contribution to overall glucose consumption is minor.

Figure 5 shows coronal sections of the parietal cortex (panels A, B, C, and D) and sagittal sections of the cerebellum (panels E and F). The cells in the cortex showing high 2-NBDG phosphorylation (A) correspond well with NeuN positive neurons (B), whereas GFAP-positive astroglia (C) showed different morphology and different distribution. Superimposed images of 2-NBDG images and immunohistochemical images could not be constructed for these regions because they lacked specific landmarks. Instead, cresyl violet staining of the cerebral cortex, which corresponds to the observed region in panels A, B, and C, is shown in panel D to facilitate cellular identification. Size and distribution of large cells in panel D, which are usually regarded as neurons, resemble those of NeuN positive cells in panel B and most of 2-NBDG accumulated cells in panel A. Small cells in panel D, astroglia, may also be observed in panel A as smaller cells with 2-NBDG accumulation, but definite

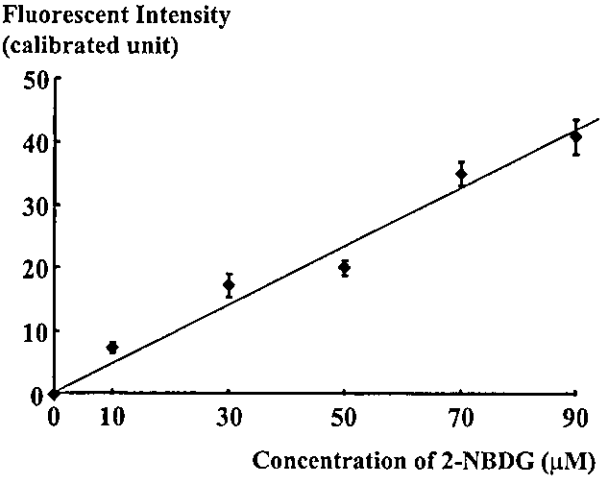

FIG. 3. Phosphorylation of 2-NBDG in astroglia. Fluorescence intensity derived from phosphorylated 2-NBDG in astroglia during 15 minutes of incubation increases proportionately with the 2-NBDG concentration in the reaction mixture. Thirty consecutive regions of interest were measured, and values are expressed as means ± SD.

confirmation was not achieved because of the lack of superimposed images. Similarly, cerebellar cells with 2-NBDG phosphorylation (E) resemble NeuN positive cells (F) in size and distribution. White matter of the cerebellum in E showed low accumulation of 2-NBDG, in good agreement with conventional 2-[^{14}C]deoxyglucose method.

2-NBDG transport across the blood-brain barrier is more limited than that of 2-deoxyglucose, and a 10-fold higher intravenous dose is required to obtain definitive images of 2-NBDG phosphorylation. Therefore, to avoid systemic effects and to obtain more precise images, 2-NBDG was infused into the cisterna magna. Sagittal sections of a cerebellar lobule are shown in Fig. 6. Panel A shows accumulated 2-NBDG, diffusely in the molecular layer and over cell bodies in the Purkinje cell layer and granular cell layer. Immunostaining of the same section for calbindin (panel B) demonstrates Purkinje cells. Panel C, a superimposed image of panels A and B, clearly demonstrates that calbindin positive Purkinje cells (arrow) all contain accumulated 2-NBDG. Magnified images (obtained with 40× objective lens) of the square regions in panels A, B, and C (obtained with 10× objective lens) are shown in panels D, E, and F, respectively. Calbindin positive Purkinje cells with 2-NBDG accumulation are indicated with thick arrows. These results are *in vivo* evidence that Purkinje cells as well as hippocampal pyramidal neurons utilize glucose as an energy substrate.

DISCUSSION

Oxidative metabolism of glucose is normally the almost exclusive source of energy in the brain, and there is considerable evidence of an interaction between energy metabolism in neurons and in astroglia. On the basis primarily of studies with cultured cells, it has been proposed that glycolytic and oxidative pathways of glucose metabolism are compartmentalized between astroglia and neurons, with glycolysis in astroglia to produce lactate, which is then exported to neurons for oxidation. (Magistretti and Pellerin, 1999; Pellerin et al., 1998). The extent of this metabolic partitioning is, however, controversial. Some question the existence of such a separation; some suggest that portioning is present to some extent but neither an absolute requirement nor complete (Itoh et al., 2003*a,b*), and some believe it to be essentially complete with glycolytic metabolism of glucose confined to astroglia and stoichiometrically coupled to glutamate/glutamine recycling (Sibson et al., 1998). Although studies with cultured cells indicate that *in vitro* they exhibit metabolic properties consistent with the proposed partitioning (Itoh et al., 2003*a,b*; Magistretti and Pellerin, 1999; Pellerin et al., 1998), the controversy persists because there has not yet been any direct examination of glucose metabolism in neurons and astroglia *in vivo*. In the present study we have used the fluorescent dye, 2-NBDG, an analogue of deoxyglucose that can be phosphorylated by hexokinase, and demonstrated for the first time to our knowledge that neurons as well as astroglia take up and phosphorylate glucose directly not only *in vitro* but also *in vivo*. At least in the hippocampus, cerebral cortex, and cerebellar lobules, glucose consumption was predominant in neurons, although low glucose phosphorylation in astroglia was also suggested. Even though the present study does not offer quantitative information on the extent of lactate utilization compared with glucose utilization in neurons, it is suggested that astroglial supply of lactate to neurons is not primary in overall energy production, based upon these findings. If astrocytes are more glycolytic than oxidative and neurons are dependent more upon lactate than glucose, then astrocytes labeled with phosphorylated 2-NBDG would be readily detectable and neuropil would be highly labeled.

It is widely reported that neurons *in vitro* consume more glucose than cultured astroglia (Brookes and Yarowsky, 1985; Itoh et al., 2003*b*; Takahashi et al., 1995). Therefore, we did not compare the glucose phosphorylation rate between neurons and astroglia *in vitro* with 2-NBDG in the present study. Although it may appear that neurons phosphorylated more glucose (155 unit/20 min) than astroglia (27 unit/20min), depending upon the fluorescent intensity results (graphs in Figs. 1 and 2), the difference in cellularity of the culture and magnification of imaging between the neurons and astroglia made it difficult to compare absolute glucose phosphorylation rate. The main disadvantage of the 2-NBDG is that it can fade in light, whereas radioactivity

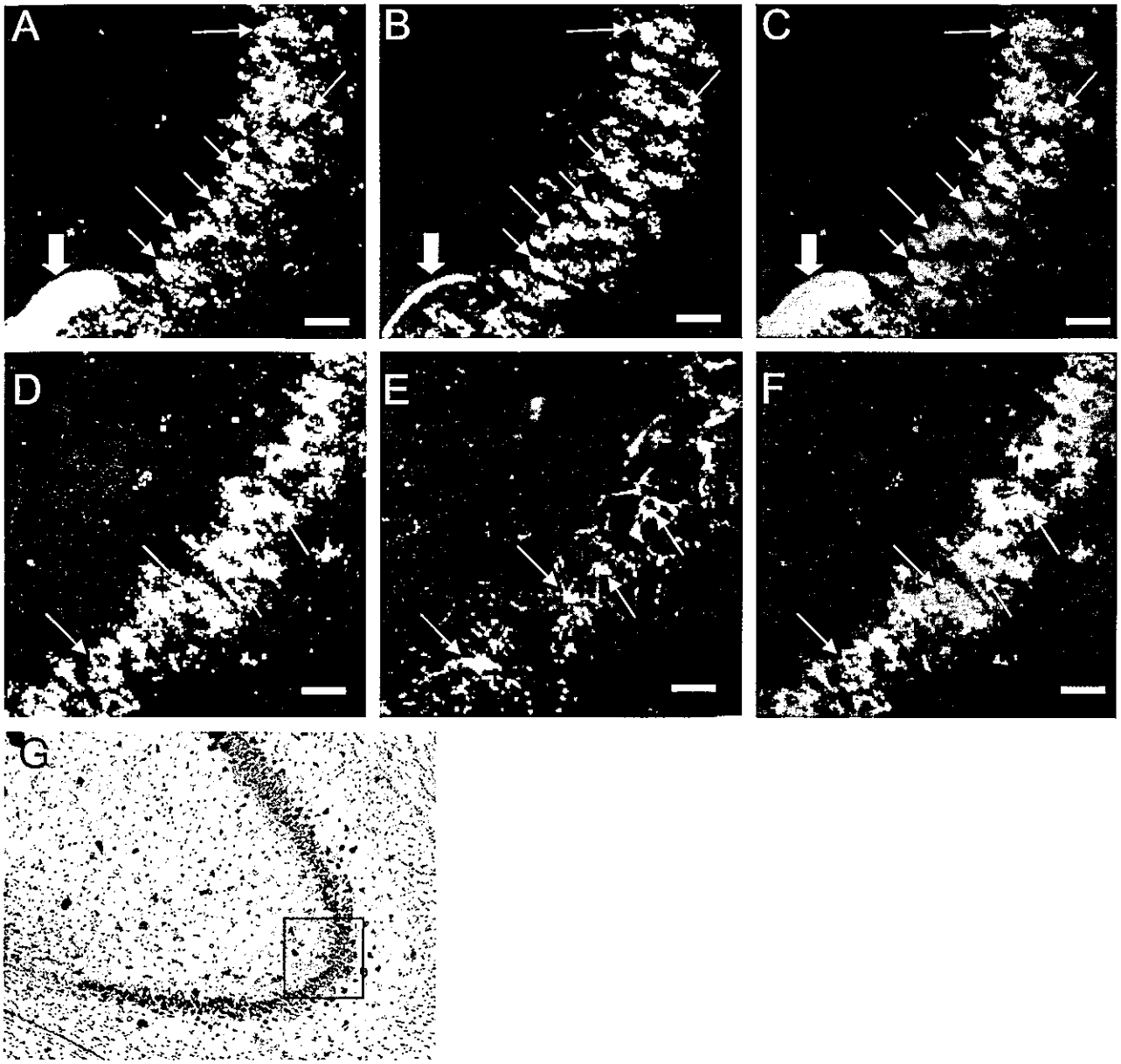

FIG. 4. Brain sections at the level of hippocampus. A to F demonstrate fluorescent images at CA3 region of hippocampus. The region of observation is indicated by a square in G (cresyl violet staining). **A:** Phosphorylated 2NBDG fluorescence in the pyramidal cell layer, mostly over cell bodies. **B:** Anti-NeuN positive pyramidal neurons in CA3. **C:** A superimposed image of A and B. It shows high agreement (yellow regions, arrows) in distribution and morphology between 2-NBDG-accumulated cells and NeuN positive neurons. Artifacts such as the one in A, B, and C (thick arrow) were used to construct overlay of 2-NBDG images and immunohistochemical images. **F:** A superimposed image of D (2-NBDG image) and E (GFAP staining). GFAP positive astroglia appear to constitute minor part of the cells with phosphorylated 2-NBDG. These cells shown in yellow (arrow) in F, however, are small in number, sparse in distribution, and different in morphology as compared with cells with 2-NBDG accumulation. The involvement of astroglia in overall 2-NBDG accumulation in F is distinctly minor compared with the predominant neuronal involvement shown as high agreement of 2-NBDG-accumulated cells and NeuN positive neurons in C. Scale bars = 50 μm.

of 2-[^{14}C]deoxyglucose, which was previously used to measure absolute glucose phosphorylation rate in cultured neurons and astroglia (Itoh et al., 2003*b*), is quite stable. Therefore, we did not further measure the absolute glucose utilization in the present study with 2-NBDG.

Among the cells with high rates of glucose phosphorylation, we successfully identified NeuN-positive pyramidal neurons in hippocampus and calbindin-positive Purkinje cells in the cerebellum by constructing superimposed images. Even though we obtained quite suggestive data that other neurons in the cerebellum and cerebral cortex also utilize glucose, they were not definitely identified because of technical difficulties. 2-NBDG and its phosphorylated derivative are water-soluble and, therefore, removed during immunostaining procedures.

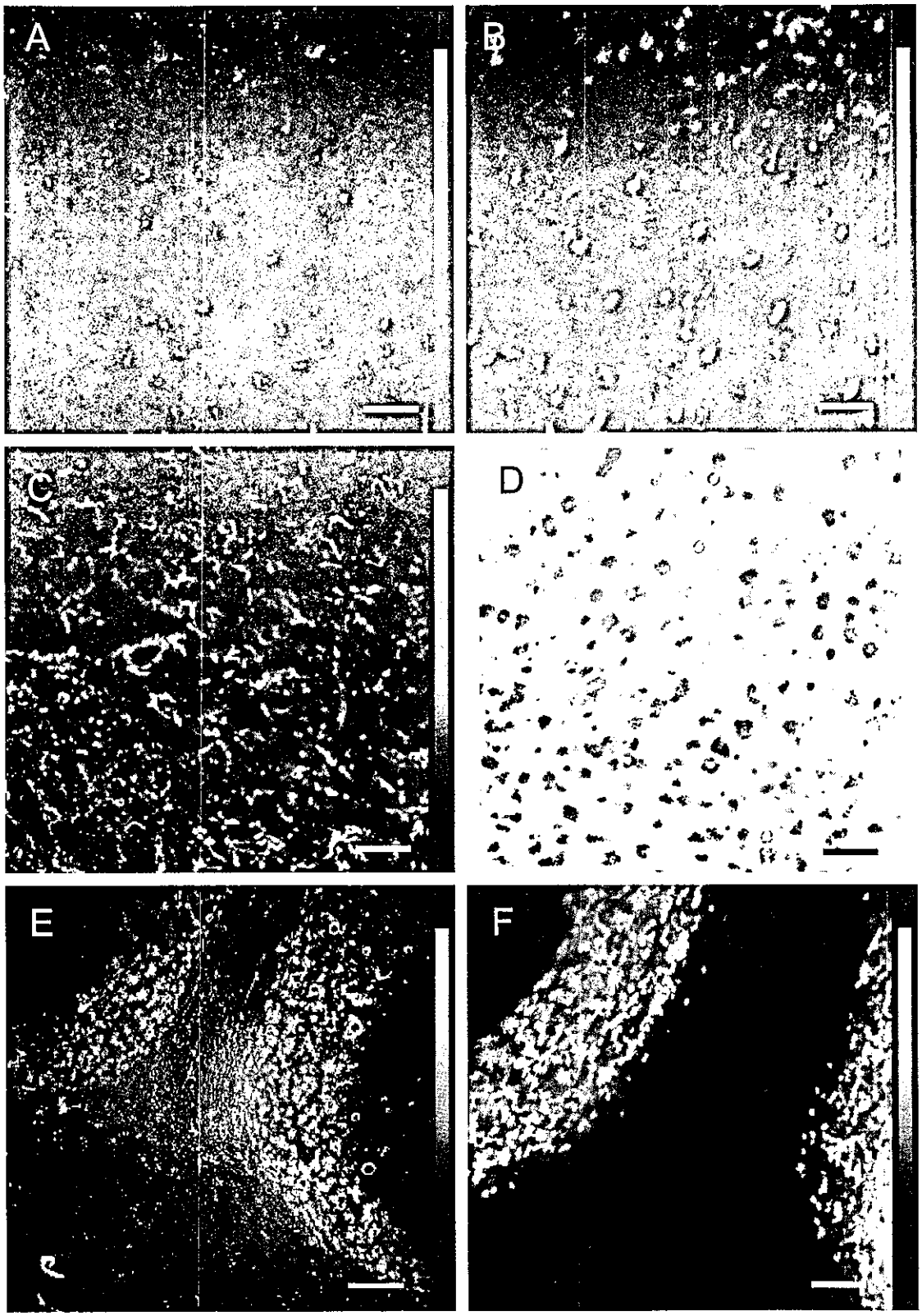

FIG. 5. Coronal sections of the parietal cortex (A, B, C, and D) and sagittal sections of the cerebellum (E and F). The cells in the cortex showing high 2-NBDG phosphorylation (A) correspond well with NeuN positive neurons (B), whereas GFAP-positive astroglia (C) show different morphology and different distribution. Size and distribution of large cells in D (cresyl violet staining), regarded as neurons, resemble those of NeuN positive cells (B) and most of 2-NBDG accumulated cells (A). Small cells in D, astroglia, may also be observed in A as smaller cells with 2-NBDG. Similarly, cerebellar cells with 2-NBDG phosphorylation (E) resemble NeuN positive cells (F) in size and distribution. Scale bars = 50 μm (A, B, C, D, and F) and 100 μm (E).

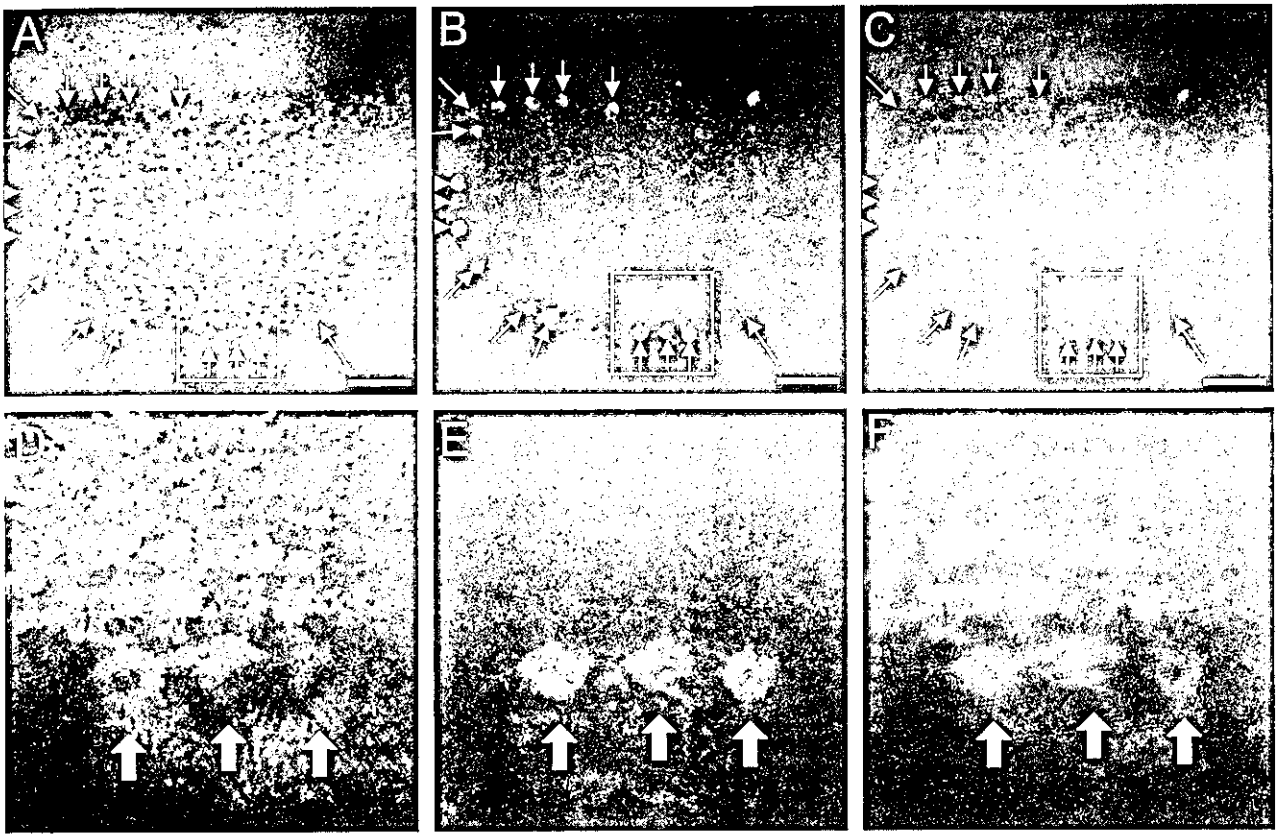

FIG. 6. Sagittal sections of a cerebellar lobule. **A:** Accumulated 2-NBDG in the cerebellum. **B:** Immunostaining of the same section for calbindin. **C:** A superimposed image of A and B. It clearly demonstrates that calbindin positive Purkinje cells (arrow) all contain accumulated 2-NBDG. **D, E, F:** Magnified images of square regions in A, B,and C (obtained with 10× objective lens) (D, E, F: obtained with 40× objective lens), respectively. Calbindin-positive Purkinje cells with 2-NBDG accumulation are indicated with thick arrows. Scale bars = 100 μm (A, B, and C).

The fluorescent 2-NBDG images and the immunohistochemical images could not, therefore, be obtained simultaneously from the same tissue sections, which, if possible, would have allowed superimposition of the two images and immunochemical identification of cells with high rates of 2-NBDG phosphorylation in all regions of the brain. We, therefore, limited our examination only to neurons in the hippocampus and cerebellum that have sufficiently unique characteristics that they could be readily identified. There are other methodological issues to be considered. It was previously reported that 50 μM 2-[^{14}C]deoxyglucose was a tracer concentration that could be used with cultured brain cells without toxic effects (Gotoh et al., 2000; Takahashi et al., 1995). Under conditions of our assay we found the 2-NBDG phosphorylation rate in astroglia to be relatively linear with respect to 2-NBDG concentration in a range extending up to 90 μM. This linearity indicates that there was no interference with the normal rate of glucose utilization in our assay with 2-NBDG. Furthermore, the rates of 2-NBDG phosphorylation in both neurons and astroglia were also linear with incubation time up to 20 minutes, indicating that we were measuring initial rates. Recently, Loaiza and colleagues (2003) reported that 2-NBDG and its analogue 6-NBDG are useful in assessing glucose transporter activity in astroglia. Compared with the rate of glucose transport, the rate of glucose phosphorylation in the brain is much slower and rate-limiting for glucose metabolism (Sokoloff et al., 1977). This is why it is essential in the assay of the rate of glucose phosphorylation with 2-NBDG to remove by washout any residual fluorescence caused by nonphosphorylated 2-NBDG.

The dose of 2-NBDG required to obtain definitive images of phosphorylation in the brain cells *in vivo* is approximately 10-fold higher than the dose of 2-[^{14}C]deoxyglucose generally used with the standard 2-[^{14}C]deoxyglucose method. The difference in required dosages probably reflects more limited blood-brain barrier transport of 2-NBDG and/or higher K_m or lower V_{max} of hexokinase for 2-NBDG than for 2-[^{14}C]deoxyglucose. Pharmacologic doses of 2-deoxyglucose are known to inhibit glucose phosphorylation (Landau et al., 1958) as well as conversion of glucose-6-phosphate to fructose-6- phosphate (Wick et al., 1957), and Horinaka and colleagues (1997) reported that 200 mg/kg (*i.e.*, 1.2 mmol/kg) of 2-deoxyglucose in rats increased cerebral

blood flow but without affecting systemic blood pressure, blood gas tensions or pH, and plasma lactate concentrations. The doses of 2-NBDG that we used (2.5 μmol/kg and 25 μmol/kg) are far below the doses of 2-deoxyglucose that have pharmacologic effects. Nevertheless, to obtain more detailed images of 2-NBDG phosphorylation while avoiding systemic side effects, we administered 2-NBDG into the cisterna magna. After 60 minutes of continuous infusion of 2-NBDG, an additional period of 60 minutes was allowed for washout of nonphosphorylated 2-NBDG from the tissues. Although full quantitative analysis of rates of glucose phosphorylation was not achieved with this method, detailed images of the distribution of phosphorylated 2-NBDG in the brain tissues and cells were obtained.

Compared with the autoradiographic 2-[^{14}C]deoxyglucose method, the fluorescent images of 2-NBDG have better spatial resolution but less quantitative information. The fluorescent images can delineate each cell with accumulation of 2-NBDG, but low accumulation of 2-NBDG is difficult to differentiate from the background intensity. Figures 4, 5, and 6 demonstrate cell bodies of neurons with high 2-NBDG phosphorylation, whereas the background surrounding the cell bodies may appear to have no fluorescence, although it should have low intensity. Thus differences in resolution and quantitative information between 2-[^{14}C]deoxyglucose method and 2-NBDG method may have resulted in apparent discrepancy in the obtained images.

It is generally believed that neuronal cell bodies have much lower rates of glucose utilization compared with the dendritic region. Because phosphorylated deoxyglucose should diffuse through cytosol of neurons, it is not surprising that cell bodies as well as dendrites are visualized with 2-NBDG method. It is because of the limitation in spatial resolution that 2-[^{14}C]deoxyglucose method can detect glucose utilization in neither single neurons nor cell bodies *in vivo*. The resolution of the original method is approximately 200 μm, which does not allow for analysis of the cellular localization of the isotope (Sokoloff et al., 1983). To improve spatial resolution of the 2-[^{14}C]deoxyglucose method, Hökfelt and colleagues (1983) modified the original technique, using [^{3}H]2-deoxyglucose, gluing the sections at −20°C, and applying emulsion with the loop technique. The images obtained with [^{3}H]2-deoxyglucose are in good agreement with those in the present study. They reported that in the hippocampus the cell body layers (pyramidal and granular layers) had high radioactivity with the majority of radioactivity located over cell bodies, whereas the fiber layers exhibited weaker activity. In their study, labeled cells were also observed in layers 2–6 in the cortex. It should be stressed that the highest densities of activity in the gray matter were seen over the cell bodies rather than neuropil in their report as well as in the present study, whereas the conventional 2-deoxyglucose autoradiographs show higher grain density over apparent neuropil, such as the stratum lacunosum moleculare of the hippocampus. Unlike the present study, Hökfelt and colleagues (1983) did not identify the cell types with high [^{3}H]2-deoxyglucose accumulation in any brain regions.

Neuropil surrounding the cell bodies in Fig. 5A did not show high accumulation of 2-NBDG. This finding, however, does not exclude the possibility that dendrites of neurons or processes of astrocytes contained phosphorylated 2-NBDG. On the contrary, *in vitro* results of the present study demonstrated that phosphorylated 2-NBDG distributes throughout cytoplasm (Figs. 1 and 2). The processes in the neuropil may not be dense enough to show 2-NBDG accumulation on this image.

Cerebrospinal fluid as well as interstitial fluid of the brain physiologically contains glucose of approximately half of the concentration found in the blood. Because no known barrier exists between cerebrospinal fluid and interstitial fluid in the brain, 2-NBDG administered in the cistern can diffuse to interstitial fluid surrounding the neurons. The present study demonstrated that phosphorylated 2-NBDG accumulated at least in some types of neurons, indicating that these neurons took up and phosphorylated glucose in the interstitial fluid. In other words, 2-NBDG was used to trace neuronal glucose uptake from the interstitial fluid and its phosphorylation. Because intracisternal administration of 2-NBDG circumvents astroglia surrounding the brain capillaries, the obtained results provide no information on supply of glucose in the interstitial fluid. The glucose in the interstitial fluid, however, should physiologically be derived from the blood, because neither astroglia nor neurons can produce glucose from any substrates to release into extracellular space (Gotoh et al., 2000). Based upon this widely accepted idea and the present results, it is suggested that neurons utilize glucose supplied from the blood. There remains a possibility that additional glucose may be supplied from the blood through astroglia to neurons without being transferred into interstitial fluid.

6-NBDG, an analogue of 2-NBDG, has been previously used to assess glucose transport in the brain *in vivo* (Shimada et al., 1994). Because they were concerned that diffusion of 6-NBDG after brain sectioning might blur the fluorescence images, these investigators used a freeze-dry method. In the present study, we thaw-dried the sections very rapidly and found that there was minimal blurring of images, which was at least insufficient to interfere with identification of the cells with high 2-NBDG phosphorylation.

The present study clearly demonstrated that neurons, at least pyramidal neurons in the hippocampus and Purkinje cells in the cerebellum, take up and utilize glucose as an energy substrate. Other neurons in the cerebral

cortex and cerebellum as well as astroglia were suggested to utilize glucose, but definite evidence was not obtained in the present study. Additional studies are required to determine the contribution of glucose metabolism to overall energy production compared with lactate utilization in neurons in general.

Acknowledgments: The authors thank Dr. Louis Sokoloff (NIMH, NIH, U.S.A.) for his critical review of the manuscript and helpful suggestions.

REFERENCES

Ball S, Bailey J, Stewart J, Vogels C, Westcott S (2002) A fluorescent compound for glucose uptake measurements in isolated rat cardiomyocytes. *Can J Physiol Pharmacol* 80:205–209

Brookes N, Yarowsky PJ (1985) Determinants of deoxyglucose uptake in cultured astrocytes: the role of the sodium pump. *J Neurochem* 44:473–479

Clarke DD, Sokoloff L (1999) Circulation and energy metabolism of the brain. In: *Basic neurochemistry: molecular, cellular, and medical aspects,* 6th ed. (Siegel G, Agranoff B, Albers RW, Fisher S, eds), Philadelphia: Lippincott-Raven, pp 637–669

Dienel G, Nelson T, Cruz N, Jay T, Crane A, Sokoloff L (1988) Over-estimation of glucose-6-phosphatase activity in brain *in vivo*: apparent difference in rates of 2-[^{3}H]glucose and [U-^{14}C]glucose utilization is due to contamination of precursor pool with ^{14}C-labeled products and incomplete recovery of ^{14}C-labeled metabolites. *J Biol Chem* 263:19697–19708

Gotoh J, Itoh Y, Kuang T, Cook M, Law MJ, Sokoloff L (2000) Negligible glucose-6-phosphatase activity in cultured astroglia. *J Neurochem* 74:1400–1408

Hökfelt T, Smith CB, Peters A, Norell G, Crane A, Brownstein M, Sokoloff L (1983) Improved resolution of the 2-deoxy-D-glucose technique. *Brain Res* 289:311–316

Horinaka N, Artz N, Jehle J, Takahashi S, Kennedy C, Sokoloff L (1997) Examination of potential mechanism in the enhancement of cerebral blood flow by hypoglycemia and pharmacological doses of deoxyglucose. *J Cereb Blood Flow Metab* 17:54–63

Itoh Y, Esaki T, Shimoji K, Cook M, Law MJ, Jehle J, Kaufman E, Sokoloff L (2003*a*) Effects of lactate transport inhibitors on cerebral glucose metabolism. *J Cereb Blood Flow Metab* 23 (S1):19

Itoh Y, Esaki T, Shimoji K, Cook M, Law M, Kaufman E, Sokoloff L (2003*b*) Dichloroacetate effects on glucose and lactate oxidation by neurons and astroglia *in vitro* and on glucose utilization by brain *in vivo*. *Proc Natl Acad Sci U S A* 100:4879–4884

Landau B, Laszlo J, Stengle J, Burk D (1958) Certain metabolic and pharmacologic effects in cancer patients given infusion of 2-deoxy-D-glucose. *J Natl Cancer Inst* 21:485–494

Lloyd P, Hardin C, Sturek M (1999) Examining glucose transport in single vascular smooth muscle cells with a fluorescent glucose analog. *Physiol Res* 48:401–410

Loaiza A, Porras O, Barros L (2003) Glutamate triggers rapid glucose transport stimulation in astrocytes as evidenced by real-time confocal microscopy. *J Neuroscience* 23:7337–7342

Magistretti PJ, Pellerin L (1999) Cellular mechanisms of brain energy metabolism and their relevance to functional brain imaging. *Philos Trans R Soc Lond B Biol Sci* 354:1153–1163

Natarajan A, Srienc F (2000) Glucose uptake rates of single *E. coli* cells grown in glucose-limited chemostat cultures. *J Microbiol Methods* 42:87–96

Pellerin L, Pellegri G, Bittar PG, Charnay Y, Bouras C, Martin JL, Stella N, Magistretti PJ (1998) Evidence supporting the existence of an activity-dependent astrocyte-neuron lactate shuttle. *Dev Neurosci* 20:291–299

Román Y, Alfonso A, Louzao M, Vieytes M, Botana L (2001) Confocal microscopy study of the different patterns of 2-NBDG uptake in rabbit enterocytes in the apical and basal zone. *Pflügers Arch* 443:234–239

Shimada M, Kawamoto S, Hirose Y, Nakanishi M, Watanabe H, Watanabe M (1994) Regional differences in glucose transport in the mouse hippocampus. *Histochem J* 26:207–212

Sibson NR, Dhankhar A, Mason GF, Rothman DL, Behar KL, Shulman RG (1998) Stoichiometric coupling of brain glucose metabolism and glutamatergic neuronal activity. *Proc Natl Acad Sci U S A* 95:316–321

Sokoloff L, Kennedy C, Smith CB (1983) Metabolic mapping of functional activity in the central nervous system by measurement of local glucose utilization with radioactive deoxyglucose. In: *Handbook of chemical neuroanatomy, vol. 1* (Björklund A, Hökfelt T, eds), Amsterdam: Elsevier, pp 416–441

Sokoloff L, Reivich M, Kennedy C, Des Rosiers M, Patlak CS, Pettigrew KD, Sakurada O, Shinohara M (1977) The [^{14}C]deoxyglucose method for the measurement of local cerebral glucose utilization: theory, procedure, and normal values in the conscious and anesthetized albino rat. *J Neurochem* 28:897–916

Takahashi S, Driscoll B, Law M, Sokoloff L (1995) Role of sodium and potassium ions in regulation of glucose metabolism in cultured astroglia. *Proc Natl Acad Sci U S A* 92:4616–4620

Wick AN, Drury DR, Nakada HI, Wolfe JB (1957) Localization of the primary metabolic block produced by 2-deoxyglucose. *J Biol Chem* 224:963–969

Yamada K, Nakata M, Horimoto N, Saito M, Matsuoka H, Inagaki N (2000) Measurement of glucose uptake and intracellular calcium concentration in single, living pancreatic β-cells. *J Biol Chem* 275:22278–22283

Yoshioka K, Oh K, Saito M, Nemoto Y, Matsuoka H (1996*a*) Evaluation of 2-[N-(nitrobenz-2-oxa-1,3-diazol-4-yl)amino]-2-deoxy-D-glucose, a new fluorescent derivative of glucose, for viability assessment of yeast Candida albicans. *Appl Microbiol Biotechnol* 46:400–404

Yoshioka K, Takahashi H, Homma T, Saito M, Oh K-B, Nemoto Y, Matsuoka H (1996*b*) A novel fluorescent derivative of glucose applicable to the assessment of glucose uptake activity of *Escherichia coli*. *Biochim Biophys Acta* 1289:5–9

脳塞栓症の治療		
基礎治療	標準治療	最新治療
1．発症後時間・重症度の把握	薬物療法　1．高張グリセロール液	1．t-PA 静脈内投与(発症 3 時間以内)
2．塞栓源の同定	2．エダラボン(発症 24 時間以内)	2．局所血栓溶解療法(発症 6 時間以内)
3．呼吸・循環の管理	3．ヘパリン(再発予防)	
4．基礎疾患の管理		

解　説

脳塞栓症は，心原性脳塞栓症と動脈原性塞栓症に分けられる．後者は，artery to artery embolism とも呼ばれ，NINDS の分類[1]ではアテローム血栓性脳梗塞に分類される．ここでは，主に心原性脳塞栓症の急性期治療にしぼって話を進める．心原性脳塞栓症の塞栓源で最も多いのは心房細動である．

標準治療

脳塞栓症は，突然発症し，皮質に及ぶ梗塞をきたすことが多い．したがって大梗塞の場合は脳浮腫の程度も強く，頭蓋内圧亢進をきたす．このような場合には，高張グリセロール(10%)静脈内投与が推奨される．グリセロールの静脈内投与は脳浮腫を改善し，脳血流量を増加させ，脳代謝を改善させる．マニトール(20%)は脳梗塞急性期に使用することを考慮してもよいが，十分な科学的根拠がない．腎障害，糖尿病の悪化に注意する必要がある．エダラボン(抗酸化薬)は，脳塞栓症急性期に脳保護作用が期待される薬剤である[2]．世界で初めて脳保護薬として認可された．発症 24 時間以内の脳梗塞患者に使用される．しかし，急性腎不全(重篤な腎機能障害を含む)の発現，および致死的転帰を来した症例が報告されており，重篤な腎機能障害のある患者には禁忌，高齢者や腎機能障害・心疾患・肝機能障害の合併例には慎重投与とされる．

ヘパリンに関する大規模な試験 International Stroke Trial (IST)[2]では，発症後 48 時間以内の脳梗塞患者 19,435 例を対象にし，第 1 群には中等量のヘパリン(12500 単位皮下注，1 日 2 回)，第 2 群には少量のヘパリン(5000 単位皮下注，1 日 2 回)，第 3 群にはヘパリンを投与せず，治療を 2 週間行い，2 週後と 6ヵ月後に死亡，脳卒中の再発，機能予後，出血合併症を調査した．その結果ヘパリンの有効性は証明されなかった．ヘパリンは虚血性脳卒中の再発を抑制するが，同程度に脳出血を発生させた．また，心原性脳塞栓症の発症後早期の再発は比較的低く，ヘパリンの使用に反対する意見もある．しかし，心房内血栓が存在するような場合には早期の抗凝固療法が必要であり，ヘパリンの適応となる症例，投与開始時期，投与量などは一定の見解が得られていない．

アメリカの Cerebral Embolism Task Force[3,4]は，心原性脳塞栓症に対する早期抗凝固療法の指針を示している．すなわち，非細菌性心原性塞栓症で発症後 24 時間以後に CT スキャンをとり，出血性脳梗塞であった場合，および出血性脳梗塞がなくても大梗塞または中等症以上の高血圧(180/100 mmHg 以上)合併例は，大出血を生じる危険性があるので早期抗凝固療法は避けるべきであり，これらの症例では抗凝固療法の開始は発症後少なくとも 7 日間は見合わせ，follow up CT を施行して開始の有無や時間を決定する．その他の症例ではすぐに抗凝固療法を開始するとする方針である．

最新治療

脳塞栓症急性期の治療のなかで，治療効果についてのエビデンスがあり，最も注目されているのが血栓溶解療法である．心原性脳塞栓は，発症後早期であればフィブリンに富む血栓であり血栓溶解療法で溶解されやすい．

▣ 血栓溶解療法(静脈内投与)

米国の NINDS の報告[5]では，発症後 3 時間以内の脳梗塞患者に t-PA(alteplase 0.9 mg/kg)かプラセボを点滴静注しその効果を検討した．患者は発症時間の明らかな症例のみとし，CT で脳出血の認められた症例，収縮期血圧が 185 mmHg 以上，拡張期血圧が 110 mmHg 以上の症例，症状が急速に回復している症例や症状が軽微のものは除外した．その結果，3ヵ月後の機能予後〔Barthel index, modified Rankin scale, Glasgow outcome scale, NIH stroke scale(NIHSS)〕が t-PA 群で有意に改善した．後遺症が軽度か全くない予後良好例が t-PA 群ではプラセボより少なくとも 30%多かった．その結果，発症後 3 時間以内の脳梗塞患者に対する t-PA の静脈内投与が，まず米国で認可された．米国での t-PA の静脈内投与が認可されて以来，

0289-0585/04/¥500/論文/JCLS

塞栓

棚橋紀夫（たなはしのりお）
慶應義塾大学講師 神経内科

標準治療のメリット	最新治療のメリット
1．中等・重症例での脳浮腫（頭蓋内圧亢進）にグリセロールは有効 2．エダラボンは抗酸化作用を有し，脳保護薬として有用性が確立されている 3．ヘパリンは再発予防に有効	1．発症3時間以内の症例で，重症でなく，早期CT所見を有さない場合にt-PA（静脈内投与）は有効 2．局所血栓溶解療法は発症6時間以内で中大脳動脈M1，M2閉塞に有効

標準療法のデメリット	最新治療のデメリット
1．グリセロールは，腎障害患者では使用できない． 2．グリセロールは糖尿病を悪化させる． 3．エダラボンは高齢者では致死的な経過をたどることがある． 4．エダラボンは腎障害・脱水・感染症・高度の意識障害のある患者には慎重投与 5．ヘパリンは，投与時期・重症度により脳出血合併の危険がある．	1．t-PAの静脈内投与は，症例選択基準を逸脱すると脳出血をきたしやすい． 2．t-PAの静脈内投与は保険適応がない． 3．局所血栓溶解療法は，静脈内投与と同様脳出血の危険性がある．

その使用経験が報告されている．プロトコール違反例（発症3時間以後に投与した症例など）にt-PAを投与すると出血性合併症がおきやすいこと，また少数例であるがアナフィラキシーショックの症例も報告されている．本邦でもt-PA（alteplase 0.6 mg/kg）を用いた発症3時間以内の脳梗塞患者に対する臨床試験が終了し，近い将来に認可される可能性がある．本邦での脳卒中治療ガイドライン[6]では，1）t-PA（保険適応外）の静脈内投与は，経験を積んだ専門医師が適切な設備を有する施設で，適応基準（脳梗塞発症3時間以内，CTで早期虚血所見がないかまたは軽微，など）を十分に充たす場合については，脳梗塞急性期の治療として有効性が期待される（グレードA）．ただし，上記の条件を満たさない場合，予後を悪化させる可能性があるため，その使用は専門的施設で行われるべきである，としている．

▣ 血栓溶解療法（経動脈内投与）

PROACT II（Prolyse in Acute Cerebral Thromboembolism II）[7]では，発症6時間以内の脳血管撮影で確認された中大脳動脈閉塞患者を対象に，動脈内にrecombinant prourokinase（r-proUK）を投与しヘパリンを併用した群と，ヘパリンのみ使用した群で無作為化比較open-label試験が行われた．その結果，r-proUKの6時間以内の動脈内投与は症候性脳出血を増加させるが，90日目の臨床結果が改善することが示された．本邦でも発症6時間以内の中大脳動脈閉塞患者を対象としたUrokinaseによる局所線溶療法の有効性を確認する無作為化比較試験（MELT-Japan）が進行中である．脳卒中治療ガイドラインでは，1）神経脱落症状を有する中大脳動脈塞栓性閉塞においては，来院時の症状が軽症から中等症で，CT上梗塞巣を認めず，発症から6時間以内に治療開始が可能な症例に対しては，経動脈的な選択的局所血栓溶解療法が推奨される（グレードB），2）しかし，上記の条件下であっても総頸動脈，あるいは内頸動脈などからの血栓溶解薬の動注は推奨されない．また，single photon emission CT（SPECT）などで残存血流量が35%未満の症例においては，経動脈的血栓溶解薬の投与は推奨されない．

血栓溶解療法は，3〜6時間とtherapeutic time windowが狭いため，適応となる症例が限られるが，著者の所属する慶應義塾大学病院に救急車で来院した脳梗塞患者では，発症2時間以内に40%が病院に到着している[8]．特に心原性脳塞栓症の患者は病院への到着時間が短い．病院に到着後に検査に時間を要する，家族からのinformed consentの取得に時間を要する点などが，血栓溶解療法の適応の阻害因子となっている．また，血栓溶解療法の適応患者の選別にMRIのperfusion weighted image（PWI）とdiffusion weighted image（DWI）のmismatch，虚血領域の残存血流量などを考慮して，血栓溶解療法の適応を決定する．

文　献
1) National Institute of Neurological Disorders and Stroke. Classification of cerebrovascular diseases III. Stroke 1990；21：637-76.
2) International Stroke Trial Collaborative Group. The International Stroke Trial（IST）：a randomized trial of aspirin, subcutaneous heparin, both, or neither among 19435 patients with acute ischemic stroke. Lancet 1997；349：1569-81.
3) Cerebral Embolism Task Force. Cardiac brain embolism. Arch Neurol 1986；43：71-84.
4) Cerebral Embolism Task Force. Cardiac brain embolism. The second report of the cerebral embolism task force. Arch Neurol 1989；46：727-43.
5) The National Institute of Neurological Disorders and Stroke rt-PA Stroke Study Group. Tissue plasminogen activator for acute ischemic stroke. N Engl J Med 1995；333：1581-7.
6) 脳卒中合同ガイドライン委員会．脳卒中治療ガイドライン2003．興和印刷：2003年5月15日発行．
7) Furlan A, Higashida R, Wechsler L, et al. Intra-arterial prourokinase for acute ischemic stroke. JAMA 1999；2003-11.
8) Yamaguchi K, Hori S, Nogawa S, et al. Thrombolysis candidates for the treatment of stroke at an emergency department in Japan. Acad Emerg Med 2002；9：754-8.

ラクナ梗塞の診断と治療

Lacunar infarction, diagnosis and treatment

棚橋 紀夫 Norio Tanahashi

慶應義塾大学医学部神経内科講師

Summary

ラクナ梗塞の診断は，臨床症状，CT，MRIによって行われるが，特にMRI拡散強調画像が責任病巣の検出に有用である。急性期治療は，発症からの時間，重症度を参考に，抗血栓療法，脳保護薬などが選択される。特に組織プラスミノーゲンアクチベーター(本邦未認可)の適応については今後注目される。慢性期には，再発予防目的に危険因子の管理・発見，抗血小板薬が適応となる。アスピリン，チクロピジン，シロスタゾールが使用可能であるが，抗血小板薬使用時には高血圧の管理が重要である。治療については，脳卒中治療ガイドライン2004が参考となる。

Key words

●ラクナ梗塞
●危険因子
●抗血栓療法
●抗血小板薬

はじめに

ラクナ(小窪，lacuna)とは，ラテン語で小さい空洞を意味し，高齢，高血圧患者の脳深部，脳幹に見出される小さい空洞よりなる小梗塞である。その大きさは小さいもので3～4mm，大きいもので1.5～2.0cmある。ラクナは多発例が多く，その約3分の1が被殻にあり，次いで橋，視床，尾状核，内包後脚，放線冠の順に頻度が多い。その他，前頭葉，側脳室外側などの大脳白質にもみられるが，大脳皮質や脊髄にはほとんど起こらない。穿通枝は側副血行をほとんどもたないので閉塞により容易に灌流領域に梗塞が生じる[1]。

1 ラクナ梗塞の定義

NINDS[2]によれば，ラクナ梗塞の定義は，神経症候を説明しうる部位に長径1.5cm未満の小梗塞を認めることとしている。さらに古典的ラクナ症候群を呈する場合には，たとえ画像上病変を認めないものもラクナ梗塞としている。

2 ラクナ梗塞の成因

ラクナの成立については，直径3～7mm程度の小さいラクナは，その部位を灌流する直径200μm以下の血管壁に生じる高血圧と関連の深い脂肪硝子変性(リポヒアリノーシス)，あるいは血管壊死(angionecrosis)による閉塞に由来するものが多い。ちなみにこのような血管病変は脳出血の成因ともなる。そのほか，穿通枝動脈の微小粥腫，主幹動脈のアテローム硬化による穿通枝入口部での閉塞(branch atheromatous disease；BAD)，心あるいは太い動脈に由来する小血栓による閉塞，稀に小動脈の解離もラクナの原因になる(図1)。したがって，機序による分類では，血栓性，塞栓性，血行力学的のいずれの可能性も有する。

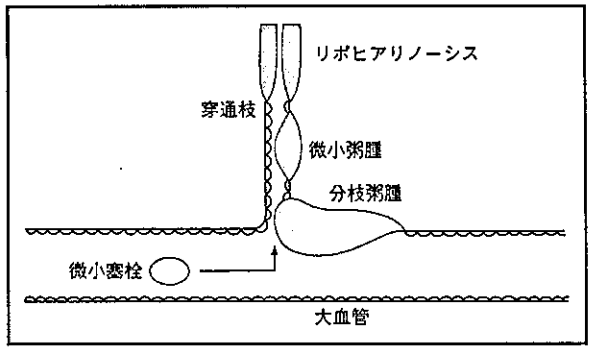

図1 ラクナ梗塞の発生機序[1]

3 ラクナ梗塞の頻度

近年，アテローム血栓性脳梗塞の増加，ラクナ梗塞の減少が指摘されているが，脳梗塞の約3分の1を占める。図2に脳梗塞急性期医療の実態に関する研究(平成12年，研究代表者：山口武典)[3]で示された脳梗塞の臨床病型別頻度を示す。

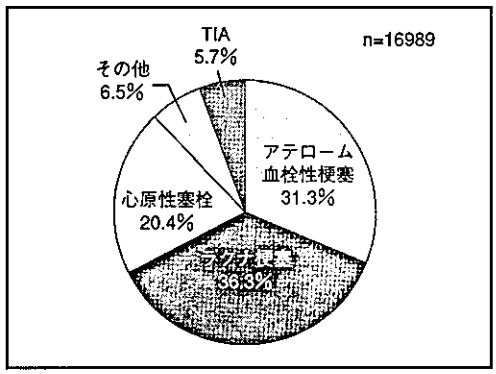

図2 脳梗塞の病型別頻度[3]

4 ラクナ梗塞の症状・予後

古典的ラクナ症候群は，pure motor hemiparesis, pure sensory stroke, ataxic hemiparesis, dysarthria-clumsy hand syndrome, sensorimotor strokeなどがある[4][5]。Pure motor hemiparesisが最も多い。Fisherは，通常ラクナでみられない症候として，失語・失行・失認などの皮質症状，単麻痺，同名半盲，健忘・意識障害・痙攣などを挙げている。ラクナ梗塞でも発症後症状の進行する進行性脳梗塞が20～30%認められる。ラクナ梗塞の予後は，きわめて良好で，脳卒中急性期患者データベース[6]の結果では，退院時(平均33日)のmodified Rankin Scaleは，0 (17.7%)，1 (41.8%)，2 (17.3%)，3 (9.3%)，4 (10%)，5 (3.0%)，6 (死亡) (0.1%)であった。

5 ラクナ梗塞の診断

MRI，CTがその診断に用いられる。ラクナ梗塞では，多発性病変が多く，MRI拡散強調画像が責任病巣の確認に有用である(図3)。ラクナ梗塞においても血管病変の確認のため頭蓋内・頭蓋外の血管病変の有無を確認する必要がある。1989年Caplan[7]は，アテローム硬化による穿通動脈の入り口の狭窄あるいは閉塞によるものをbranch atheromatous disease(BAD)と提唱した。梗塞巣は15mmを超えるgiant lacuneを呈することが多い。進行性脳梗塞になりやすく，治療にもかかわらず症状の進展を阻止できない例も多い。BADはNINDSの臨床病型のラクナ梗塞とアテローム血栓性脳梗塞の間に位置する病態と考えられる。

6 ラクナ梗塞の急性期治療

ラクナ梗塞の急性期治療は，発症後の時間，重症度，